Characterization of Methyl Viologen in the Channels of Zeolite L

Brian Hennessy,[†] Silke Megelski,[†] Claudia Marcolli,[†] Valery Shklover,[‡] Christian Bärlocher,[‡] and Gion Calzaferri*[,†]

Department of Chemistry and Biochemistry, University of Berne, Freiestrasse 3, CH-3000 Bern 9, Switzerland, and Laboratory of Crystallography, ETH-Zentrum, CH-8092 Zürich, Switzerland

Received: December 2, 1998; In Final Form: February 23, 1999

The degree of exchange of methyl viologen (MV^{2+}) within the channels of zeolite L microcrystals was determined as a function of the amount of MV^{2+} added to an aqueous zeolite L suspension. Care was taken to remove molecules that have been adsorbed on the outer zeolite surface. Thus, the obtained values for the maximum occupation probability per unit cell are 0.78 for the commercial and 0.85 MV^{2+} for the self-synthesized potassium zeolite L for which the equilibrium constant was found to be in the order of 10^4 at room temperature. Adsorption isotherms and BET results show that the self-synthesized zeolite has a larger specific surface area as well as a larger and, thus, more accessible pore volume for the MV^{2+} than the commercial sample. IR spectra of very thin layers on ZnSe in high vacuum and Raman spectra at ambient conditions of MV^{2+}−L zeolite at different loading levels are presented. They are compared with a $MVCl_2$−KBr pellet and MV^{2+}−Y zeolite spectra. The MV^{2+}−L zeolite spectra indicate weak interactions between the MV^{2+} and the zeolite framework. They also indicate that the two pyridyl rings of the intercalated MV^{2+} are twisted. It was found that framework vibrations of the zeolite can be used as an *internal standard* for fast and nondestructive determinations of the MV^{2+} loading. Raman spectra are better suited for this purpose than IR. The reason for this is that the IR intensities of the zeolite framework vibrations at about 1050 cm^{-1} are much higher than those for all MV^{2+} modes, while the only strong zeolite framework Raman band at about 500 cm^{-1} is narrow and well-isolated and of similar intensity to the relevant MV^{2+} signals at high loading. On the basis of Rietveld refinement of X-ray data and molecular modeling, a model of the MV^{2+} location in the channels of zeolite L is proposed. The MV^{2+} lies along the channel wall, and the angle between the main MV^{2+} axis and the *c*-axis of the zeolite is 27°.

1. Introduction

Zeolites are appealing inorganic microporous frameworks that possess a large variety of well-defined internal structures such as uniform cages, cavities, or channels.[1,2] A useful feature of zeolites is their ability to readily intercalate molecular guests within the intravoid space. The capacity of the zeolite framework to adopt an ordered geometrical arrangement of the intercalated molecules is used for the design of antenna systems[3−8] or charge-transfer complexes,[9,10] where either the donor or the acceptor molecules are incorporated within the zeolite framework. Systems where the methyl viologen dication MV^{2+} features as a guest molecule and an electron acceptor within a zeolite have attracted much interest.[11−20] The zeolites used as hosts have, thereby, mostly been zeolites L, Y, and ZSM-5. The parallel, linear channels of zeolite L make it well-favored for intercalation of molecules within it in order to obtain microcrystals with pronounced anisotropic properties.[4,21,22] An important, recurring question that arises in the study of intercalated molecules is one regarding the location and number of the guests trapped in the voids of the host. Because of their length, dyes, such as thionine,[22] pyronine, oxonine,[3,5,6] resorufine,[23] and others,[4] align along the cylindrical axis of the channels of zeolite L. This is different for MV^{2+}. Its size is such that it has a chance to arrange into another position. Three possible orientations that can be imagined, considering the dimensions of MV^{2+}, are illustrated in Scheme 1. Some conflict is also seen in the literature regarding the values of exact loading levels and methods used to determine them for MV^{2+} within zeolite L. Indeed, different values for the maximum occupation of MV^{2+} within zeolite L have been quoted.[11,15,16] This may be due to the fact that it is necessary to distinguish between molecules that have been adsorbed on the outer surface of the zeolite microcrystals, eq 1, and molecules that have been intercalated, eq 2, as has been discussed in some detail for thionine, methylene blue, and ethylene blue.[22,4]

SCHEME 1: Different Spatial Configurations to Be Considered for MV^{2+} in the Channels of Zeolite L

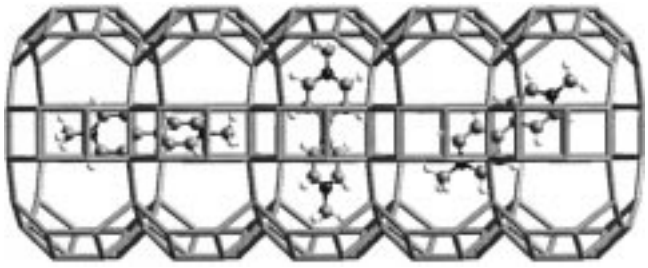

$$y\mathrm{MV}^{2+} + (\mathrm{K}^+)_n\mathrm{Zeol{-}L} \rightleftarrows (\mathrm{K}^+)_{n-2y}\mathrm{Zeol{-}L}[(\mathrm{MV}^{2+})_y]_{\mathrm{ads}} + 2y\mathrm{K}^+ \quad (1)$$

* To whom correspondence should be addressed: Tel ++41 31 631 4226; E-mail calza@solar.iac.unibe.ch.
† University of Bern.
‡ ETH-Zentrum.

10.1021/jp984573y CCC: $18.00
Published on Web 04/07/1999

$$MV^{2+} + (K^+)_m\text{Zeol}-L \rightleftarrows (K^+)_{m-2}\text{Zeol}-L(MV^{2+})_{\text{channel}} + 2K^+ \quad (2)$$

Equilibrium 2 can also be expressed in the sometimes more convenient form:

$$MV^{2+}{}_S + 2K^+{}_Z \rightleftarrows MV^{2+}{}_Z + 2K^+{}_S \quad (2')$$

where $MV^{2+}{}_S$ and $K^+{}_S$ are cations in the aqueous suspension (S) and $MV^{2+}{}_Z$ and $K^+{}_Z$ are cations intercalated in the zeolite channels (Z). The quality of the microcrystals characterized by the specific pore volume is important and must be considered, as we will show. We have, therefore, studied carefully the loading of a commercial and of a self-synthesized zeolite L with MV^{2+} present in different amounts in aqueous zeolite suspensions. The MV^{2+} loaded zeolite L samples, which we name $MV^{2+}-L$ zeolite, were investigated with IR and Raman spectroscopy to obtain information on the zeolite−guest relationship and to study the question whether zeolite framework vibrations can be used as an internal standard for quantitative MV^{2+} concentration measurements. This also made it necessary to examine the location of the MV^{2+} in zeolite L. This problem was investigated by means of X-ray structure refinement and by molecular modeling.

2. Experimental Section

2.1. Physical Measurements. *UV−Vis Absorption Spectra*. These were recorded using a Perkin-Elmer Lambda 14 spectrophotometer with 10 mm path length quartz cuvettes in all measurements. For the absorption measurements of zeolite L suspensions in water (consisting of 6.7×10^{-4} g of zeolite L per mL of water, which corresponds to approximately 4×10^8 zeolite microcrystals per mL), the spectrophotometer was equipped with an integrating sphere (Labshere RSA-PE-20).

IR and Raman Measurements. The IR spectra were recorded on a Bomem DA3 FTIR spectrometer with a built-in high vacuum cell,[24] allowing spectra to be recorded under a dynamic vacuum of the order of 10^{-6} mbar. The interferometer was equipped with an IR source, a KBr beam splitter, and a liquid-nitrogen-cooled MCT detector. Measurements were taken with a resolution of 2 cm^{-1}. For quantitative IR measurements, the normalization to the characteristic antisymmetric $\nu_{as}(T-O-T)$ peak was done by adjusting its height between 850 and 1350 cm^{-1} in each case to the same value, and then the area of the relevant MV^{2+} peak was calculated. The Raman measurements were performed with the Bomem Raman accessory of the same spectrometer. The interferometer was equipped with a quartz beam splitter and a liquid-nitrogen-cooled InGaAs detector. The continuous-wave Nd^{3+}:YAG laser (Quantronix model 114) was run in the transverse electromagnetic mode TEM_{00} at 9395 cm^{-1}. Rayleigh scattering was blocked by three holographic super notch filters in a 6° angle position. A 2 mm thick anodized aluminum plate with a 2 mm diameter hole into which the probe was slightly pressed served as a sample holder. The spectra were measured using 1024 scans with a resolution of 4 cm^{-1}, and blackbody radiation correction was applied to each spectrum. For quantitative Raman measurements, the normalization to the $\delta(O-T-O)$ peak was done by adjusting its height between 480 and 530 cm^{-1} in each case to the same value and then calculating the area of the relevant MV^{2+} peak.

Specific Surface Area Measurements. Adsorption isotherms were measured with the Sorptomatic 1990, including Krypton unit from CE-Instruments, using nitrogen as adsorbate at ~77 K in the range of relative partial pressure p/p_0 from 10^{-4} to 1.

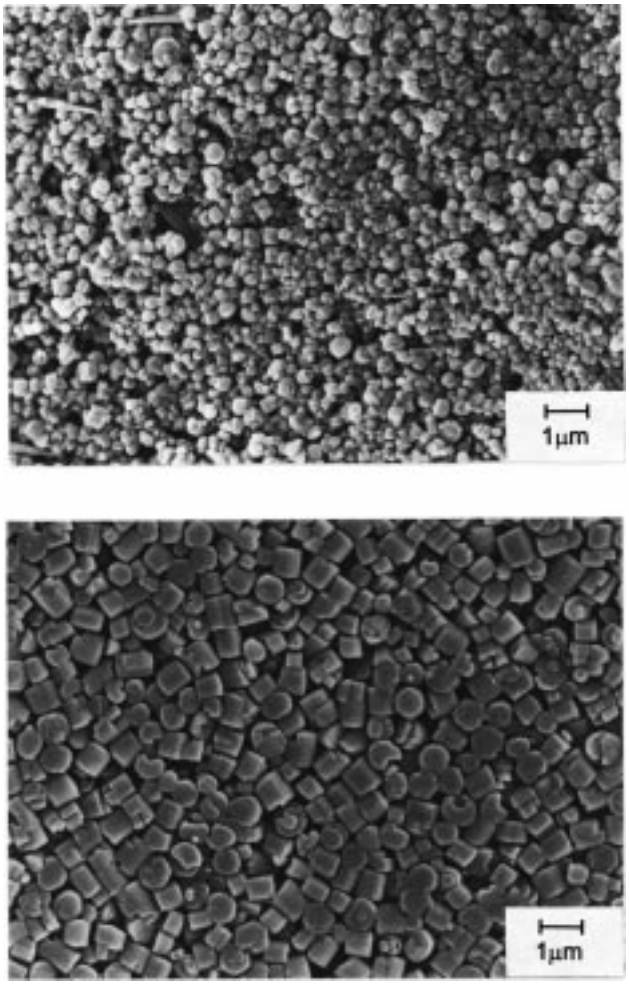

Figure 1. Scanning electron microscopy pictures of the commercial (on top) and the self-synthesized (on bottom) zeolite L samples.

The zeolite samples were degassed in an oven with a vacuum port at a rate of 0.5 K/min up to 573 K and was left for several hours at this temperature under vacuum until the residual pressure was $<10^{-4}$ mbar. To obtain the weight of dried zeolite, the empty degassed sample buret and the degassed sample buret containing the zeolite were weighed and compared. To evaluate the data, we used the software package of Sorptomatic 1990 as well as the Milestone 200 Physisorption Software Advanced Data Processing.

2.2. Materials. Zeolite L, with the stoichiometry $K_9(SiO_2)_{27}(AlO_2)_9 \cdot 21H_2O$ ($M_w = 2883$ g/mol), was synthesized using silica (AEROSIL-Dispersion, K330; Degussa), $Al(OH)_3$ (Fluka, purum), and KOH (Fluka, Biochemika) by a similar procedure as described in refs 3 and 5. The commercial zeolite Linde-type L was obtained from Union Carbide, molecular sieves type ELZ-L. Before use, the commercial zeolite L with the stoichiometry $K_6Na_3(SiO_2)_{27}(AlO_2)_9 \cdot 21H_2O$ was ion exchanged for 24 h in a 1 M KCl aqueous solution at 50 °C (typically, 1 g of zeolite in 100 mL) to ensure that all exchangeable ions were K^+ and to remove exchangeable impurities, such as an extra framework iron. The exchanged zeolite was washed several times with double-distilled water and dried overnight at about 75 °C. The completion of the exchange was verified by elemental analysis. The size of the commercial zeolite was ca. 0.2 μm; the self-synthesized consisted of cylinders with lengths and diameters of ca. 0.5 μm (see Figure 1). Methyl viologen dichloride, $MVCl_2$ (1,1′-dimethyl-4,4′-bipyridinium dichloride, Fluka Chemicals, Switzerland) was used without further purification. The extinction coefficient of methyl viologen at $\lambda_{max} = 257$ nm ($\epsilon =$

20 700 M^{-1} cm^{-1}) reported by Watanabe and Honda[25] was used in all subsequent measurements to determine the concentration of the MV^{2+} containing solutions.

2.3. MV^{2+} Exchange Isotherm and Preparation of MV^{2+}−L Zeolite. To 1 g of zeolite L, which was suspended in 100 mL of double-distilled water, different amounts (between 5 and about 1000 mg) of $MVCl_2$ were added. Intercalation of MV^{2+} into zeolite L is fast and almost completed within half an hour. However, to make sure that equilibrium 2 was fully established, the suspension was stirred for 24 h at room temperature. Since we were interested in the exchange isotherm and the loading with respect to the intercalated MV^{2+}, we proceeded as follows before analyzing the material: the 1 g exchanged samples were washed with 45 mL portions of double-distilled water by vigorous shaking (ca. 1 min), dispersed ultrasonically for ca. 1 min, and then centrifuged. The washing procedure was typically repeated two to three times until the MV^{2+} concentration in the supernatant solution was observed to remain in the order of 10^{-6} M. Each sample was then washed with *n*-butanol until no further trace of MV^{2+} could be detected by UV spectroscopy. For the self-synthesized samples, the ion exchange and washing procedure were scaled down by a factor of 20. The samples were then dried at 75 °C for 24 h. To quantify the amount of MV^{2+} actually intercalated inside the zeolite L channels, the zeolite framework was destroyed using hydrofluoric acid (48% w/v) and the MV^{2+} content was then determined by UV spectroscopy. Typically, 10 mg of a zeolite sample was accurately weighed and 1 mL of HF was added. The sample was then thoroughly shaken until the zeolite was completely dissolved, and a clear solution was obtained. The solution was neutralized with a 4 M NaOH solution and made up to 50 mL with double-distilled water. The MV^{2+} loading (occupation probability) p is defined as

$$p = \frac{\text{number of molecules intercalated}}{\text{number of sites available}} = \frac{n_{MV^{2+}}}{n_s} \qquad (3)$$

where the number of sites n_s available in zeolite L for MV^{2+} corresponds to the number of unit cells because of the size of MV^{2+}. Since the molecular weight of the zeolite changes only slightly upon exchange with MV^{2+}, n_s was calculated as follows

$$n_s = \frac{W_Z}{2883\ \text{g/mol}} \qquad (4)$$

where W_Z is equal to the amount of zeolite used in the analysis. The MV^{2+}−Y zeolite samples were prepared as described in ref 20.

2.4. Sample Preparation for Infrared and Raman Spectra. *IR Spectra.* Thin or thick layers of MV^{2+}−L zeolite suspensions were prepared on ZnSe window disks of 8 mm diameter and 1 mm thickness otherwise KBr pellet samples were used.

Thin Layers. Thirty microliters of a suspension consisting of 50 mg MV^{2+}−L zeolite in 10 mL of double-distilled water was delivered onto the center of the ZnSe disk, and the sample was left to dry slowly overnight. The amount of zeolite used results in samples of 1.5 μm thickness, corresponding to ca. 7.5 layers of zeolite grains, and yields IR spectra where the intense antisymmetric T−O−T vibration ν_{as}(T−O−T) is not saturated.

Thick Layers. For measurement of spectra with a saturated ν_{as}(T−O−T) peak, thicker samples had to be prepared. The same suspension concentration was used as for thin layers but 90 μL was delivered onto each side of the ZnSe plate, thus giving a total of ca. 45 layers of zeolite grains.

TABLE 1: Unit Cell Constants of the Zeolite L and MV^{2+} Loaded Zeolites MV^{2+}-L, Refined Using LATCON Program

zeolite	*a* (Å)	*c* (Å)	*V* (Å^3)
commercial	18.372(1)	7.5182(7)	2917.6(6)
self-synthesized	18.341(1)	7.5191(7)	2910.5(6)
MV^{2+} commercial	18.4002(7)	7.5265(6)	2207.3(2)
MV^{2+} self-synthesized	18.355(1)	7.5300(7)	2196.9(7)

TABLE 2: Crystallographic Data for MV^{2+}−L

Data Collection		
diffractometer		STOE, Debye−Scherrer mode,with PSD
sample holder		0.5 mm capillary
wavelength		Cu Kα_1
2θ range (°2θ)		4.0−97.0
step size (°2θ)		0.02
time per step		480 s
Refinement		
space group		*P*6/*mmm*
a (Å)		18.3885(2)
b (Å)		7.5448(1)
number of observations		4534
number of contributing reflections		417
number of geometric "observations"		134
SiAl−O	prescribed: 1.64(1) Å	7
O−SiAl−O	prescribed: 109.5(10)°	10
SiAl−O−SiAl	prescribed: 145(8)°	6
MV^{2+} molecule		111
number of structural parameters		91
number of profile parameters		8
$R_{exp} = [(N - P1 - P2)/\sum wy^2(\text{obs})]^{1/2}$		0.038
$R_{wp} = [\sum w[y(\text{obs}) - y(\text{calc})]^2/\sum wy^2(\text{obs})]^{1/2}$		0.116
$RF = \sum\|F(\text{obs}) - F(\text{calc})\|/\sum F(\text{obs})$		0.071

KBr Pellets. Methyl viologen dichloride ($MVCl_2$) was measured as a KBr pellet of 14 mm diameter and was prepared by grinding together 0.076 mg of $MVCl_2$ with 200 mg of KBr and pressing it under 5 ton pressure for 10 min.

Raman Spectra. For measurement of the Raman spectra, a 2 mm thick anodized aluminum plate with a 2 mm diameter hole into which the probe was slightly pressed served as sample holder.

2.5 X-ray Powder Diffraction Study. The data collection from the unloaded zeolite L and from MV^{2+}−L zeolite samples was performed using the STOE automated powder diffractometer system (Debye−Scherrer scan mode, a small position sensitive detector). The unit cell parameters were refined using the LATCON program with 18 reflections in the 2Θ range of 11−30°; see Table 1. The refinement of the powder diffraction data was performed using XRS-82 systems of programs.[26] Further details of the data collection and the crystallographic data are given in Table 2.

3. Results

While many experiments can be carried out with commercially available zeolite L, there are limitations to its use because of impurities that can, for example, severely affect the stability of intercalated organic molecules and their luminescence quantum yield. Furthermore, it is often interesting to control the morphology of the microcrystals as has been shown recently.[3−6,27] Most of the experiments reported herein have, therefore, been carried out with self-synthesized zeolite L as well as with the commercial material. We only specify the type of zeolite used in cases where necessary. A comparison of the morphology is reported in Figure 1. It illustrates the difference in size distribution and morphology of the commercial product and the material prepared by us. If not stated otherwise, the exchangeable cations are always K^+.

3.1. MV^{2+} Exchange Isotherm and Maximum Loading. The extent of surface coverage is normally expressed as the fractional coverage Θ:[28]

$$\Theta = \frac{\text{number of adsorption sites occupied}}{\text{number of adsorption sites available}} \quad (5)$$

The exchange degree θ has been defined with respect to exchangeable cations, which is 3.6 per unit cell for zeolite L, since for zeolite L only the cations belonging to the main channel can be exchanged for steric reasons:[21,22]

$$\theta = \frac{\text{number of cations exchanged per unit cell}}{\text{number of exchangeable cations}} \quad (6)$$

Since this definition does not distinguish between molecules that have been adsorbed at the outer surface of the zeolite microcrystals (eq 1) and molecules that have been intercalated (eq 2), it is convenient to use the term occupation probability p as defined in eq 3, which uniquely refers to sites located inside the cavities of the microcrystals.[3,5,6,23] In the present study, we are interested in the number of intercalated MV^{2+} per unit cell p as a function of MV^{2+} added to the zeolite L suspension at room temperature. This means that we are interested in the exchange isotherm with respect to the equilibrium 2. The equilibrium constant for this reaction is expressed in terms of concentrations in eq 7 since our knowledge regarding activities in the zeolite is not sufficient to do it otherwise, and we know from eq 37 of ref 29 that it depends on the occupation probability. We have also observed that the value of K depends significantly on the counterion. At room temperature, we have measured the following values: $K = 1.7 \times 10^6$, 1.5×10^5, 1.3×10^4, and 6.6×10^3 for $M^+ = Li^+$, Na^+, K^+, and Cs^+, respectively. The difference of the equilibrium constants is related to the different affinity of zeolite L toward the different alkali cations (see Table 20 of ref 30).

$$K = \frac{[MV^{2+}{}_Z]\,[M^+{}_S]^2}{[MV^{2+}{}_S]\,[M^+{}_Z]^2} \quad (7)$$

During the ion exchange process, a certain amount of MV^{2+} is not ion exchanged but considered to be adsorbed merely on the outer surface.[15] Studying the development of the washing procedure with double-distilled water as explained in the Experimental Section to ensure removal of any surface adsorbed MV^{2+}, we found that most of the adsorbed MV^{2+} are removed during the first two washing steps. After four steps, the concentration of MV^{2+} in the supernatant solution is seen to remain in the order of 10^{-6} M. It slightly diminishes further because of the ion exchange of MV^{2+} with H^+ of the water, a factor which starts to become important at this point. Water as a solvent is, therefore, replaced by *n*-butanol, and after three further washing steps, no further traces of MV^{2+} can be detected in the supernatant washing solution. This procedure leads to the quantitative removal of all adsorbed MV^{2+} molecules, while the intercalated ones remain within the zeolite L channels (see also ref 23). We found that washing a $MV^{2+}-L$ zeolite sample as described in the Experimental Section with n-butanol can make up to a 7% difference to the value of the occupation probability. Figure 2 shows the determined occupation probability values of MV^{2+} within a self-synthesized and commercial zeolite L plotted as a function of $C_{MV^{2+}}$, which is the amount of MV^{2+} per unit cell of zeolite L initially present in the suspension. Both curves are steep at low loading as expected from the large equilibrium constant K for reaction 2. The two curves coincide at low loading within the experimental error. Once about half of the available sites are occupied, however, a significant difference is observed between the two materials. Both curves level off above a critical concentration, which means that saturation is reached. From this graph, we conclude that the maximum occupation probability corresponds to 0.78 MV^{2+} per unit cell for the commercial and 0.85 for the self-synthesized zeolite sample. The literature values for the maximum occupation probability vary between 0.7 and 1;[11,15,16] however, in some of these measurements, little effort was taken to distinguish between molecules that were intercalated and molecules that were adsorbed merely on the outer surface of the zeolite. The higher loading reached for the self-synthesized material can be understood by the better crystallinity of the microcrystals shown in Figure 1, a conclusion which is supported by the specific surface area measurements reported in section 3.4.

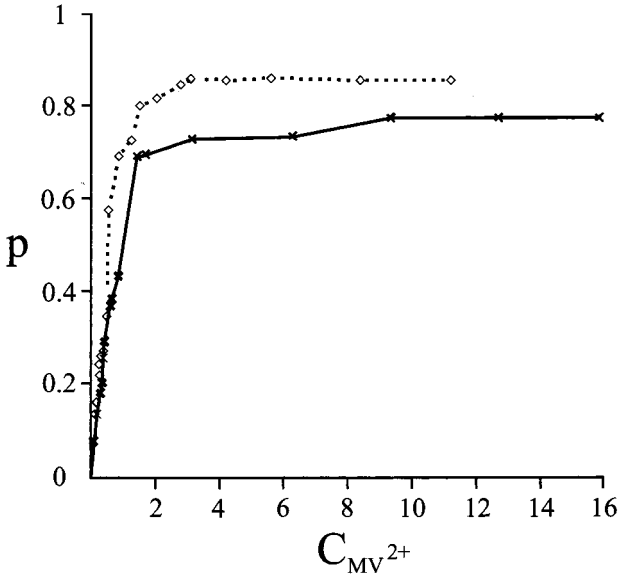

Figure 2. The occupation probability p of the $MV^{2+}-L$ zeolite as a function of $C_{MV^{2+}}$, which is the number of moles of MV^{2+} per mole of zeolite L unit cells present in the aqueous suspension. Experiments with self-synthesized zeolite are indicated by diamonds (◇) and experiments with commercial zeolite by crosses (X).

3.2. Infrared and Raman Spectra of $MV^{2+}-L$ Zeolite. Infrared and Raman spectra of molecule-loaded zeolites are used for quantitative and qualitative analytical purposes as well as for investigating the influence of the zeolite exerted on the intercalated species. We have recently shown that for very thin zeolite layers coated on ZnSe wafers, quantitative information can be obtained by using the characteristic antisymmetric ν_{as}-(T−O−T) band, T = Si or Al, as an internal standard.[31] If a similar procedure works for $MV^{2+}-L$ zeolite samples, then this could be used as an analytical tool. We begin by comparing the IR spectra of an unloaded zeolite L sample as a thin layer on ZnSe in high vacuum and of $MVCl_2$ in a KBr pellet in Figure 3. From this it is obvious that most of the information in these spectra lies below 1800 cm^{-1}. The water bending and the broad water stretching vibrations at about 1645 and 3400 cm^{-1} usually present in zeolite spectra are hardly visible. This is due to the fact that thin zeolite layers lose their water very fast under high vacuum even at room temperature as has been described recently.[31,32] We conclude that it is reasonable to restrict all further discussion to the spectral range between 550−1800 cm^{-1}.

The relative intensities of the IR active vibrations of the zeolite L framework and those of the MV^{2+} are illustrated in

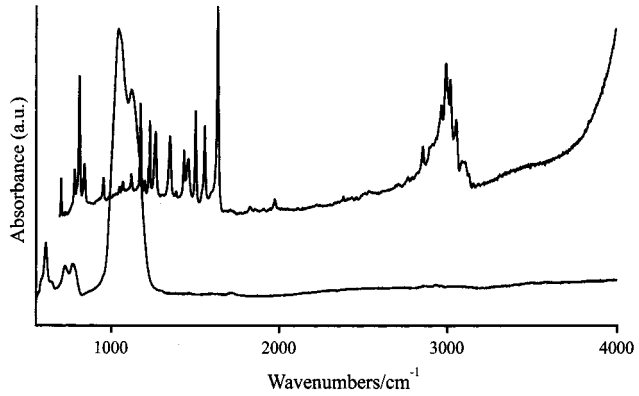

Figure 3. Overview of a thin layer unloaded zeolite L IR spectrum in high vacuum (below) and of $MVCl_2$ in a KBr pellet (above).

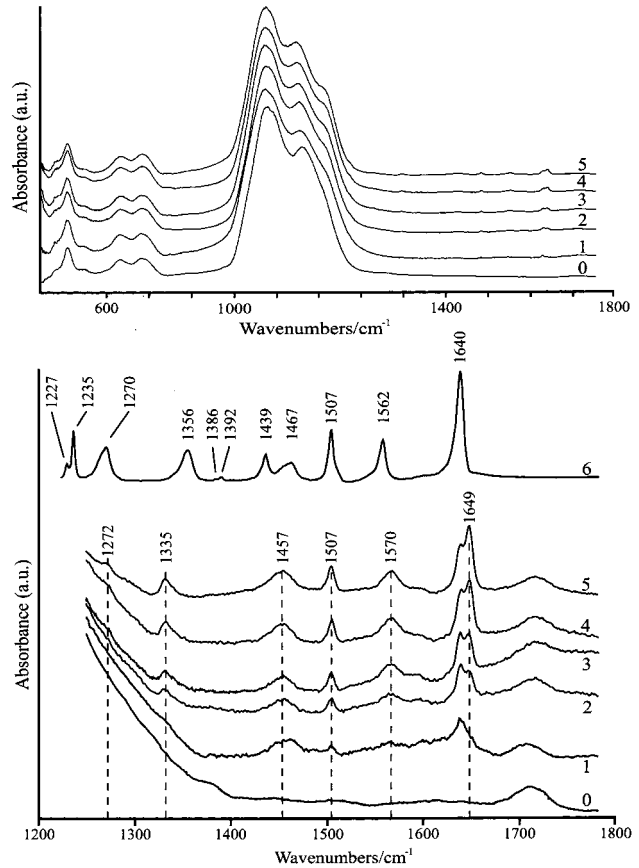

Figure 4. Above: IR absorption spectra of MV^{2+}−L zeolite at different loadings. The numbers 0, 1, 2, ..., 5 refer to $p = 0$, 0.27, 0.41, 0.52, 0.62, and 0.72, respectively. Below: Enlargement of the IR absorption spectra 0 to 5 shown above and 6 of a $MVCl_2$−KBr pellet between 1220 and 1800 cm^{-1}.

Figure 4, where spectra of MV^{2+}−L zeolite samples with different occupation probability values ranging from $p = 0$ to $p = 0.72$ are shown. We see that the spectra are dominated by the features from the zeolite framework, mainly the very intense antisymmetric stretching vibrations at about 1050 cm^{-1}. The comparison of the thin MV^{2+}−L zeolite layer bands with those of the $MVCl_2$−KBr pellet in the enlargement of the 1250−1800 cm^{-1} region illustrates that many bands belonging to the intercalated MV^{2+} are well-resolved. It is also observed that measurements become difficult at low loading. Most bands show only small shifts and some broadening with respect to those observed in the $MVCl_2$−KBr pellet spectrum. The 1467 and 1439 cm^{-1} absorptions, however, merge into one relatively broad feature, and the weak 1386 and 1392 cm^{-1} bands could not be detected at all in the MV^{2+}−L zeolite layers. The 1270 and the 1235 cm^{-1} bands appear as weak features, the latter only as a shoulder, which is not shown. The other MV^{2+} vibrations between 1240 and 900 cm^{-1} are buried under the intense zeolite ν_{as}(T−O−T) bands. Below 800 cm^{-1}, only two weak signals at 831 and 817 cm^{-1} could be detected, as illustrated in Figure 5. We tentatively correlate them with the 846 and the 815 cm^{-1} $MVCl_2$−KBr pellet bands. The situation is different for the Raman spectra. The zeolite framework gives rise to only weak Raman signals as illustrated in Figure 6. These spectra are therefore dominated by the MV^{2+} peaks. The only strong feature of the zeolite comes from the framework vibration at 500 cm^{-1}.

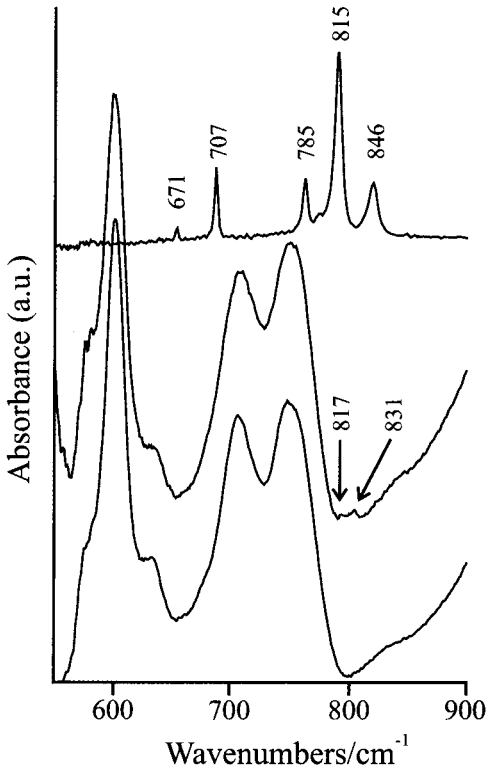

Figure 5. Enlargement of the IR spectra of bare zeolite L (below), of MV^{2+}−L zeolite at high loading ($p = 0.72$) (middle), and of a $MVCl_2$−KBr pellet (above) between 550 and 900 cm^{-1}.

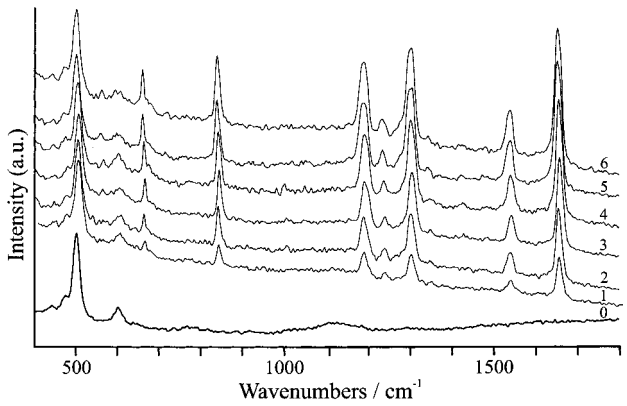

Figure 6. FT-Raman spectra of MV^{2+}−L zeolite at different loadings. The numbers 0, 1, 2, 3, 4, 5, and 6 refer to $p = 0$, 0.27, 0.41, 0.52, 0.62, 0.72, and 0.74, respectively.

The IR and Raman frequencies relevant for this work are collected in Table 3. The assignment of the MV^{2+} bands is based on comparisons with data reported in the literature.[33−42]

To test which of the two IR bands of MV^{2+}−L zeolite, 1649 and 1640 cm^{-1}, belongs to the MV^{2+} and which is caused by

TABLE 3: Vibrational Frequencies of MV^{2+}−L Zeolite[l]

IR (cm^{-1})		Raman (cm^{-1})	assignment		
MV^{2+}−L zeolite	$MVCl_2$ KBr pellet[a]	MV^{2+}−L zeolite	MV^{2+}	water	zeolite
		1651 s	8a ν_{ring}		
1649 s	1640 vs		8a ν_{ring}		
1640 s				δ (H_2O)	
1570 w	1562 m		19a ν_{ring}		
		1538 m	19a ν_{ring}		
1507 m	1507 m		8b $\nu_{ring} + \delta_{CH}$		
1457 m	1467 m		19b $\nu_{ring} + \delta_{CH}$		
	1439 m		δ $(CH_3)_{as}$[b]		
	1392 w		δ $(CH_3)_{sym}$		
	1386 vw		unassigned		
1335 w	1356 m		14 ν_{ring}[c]		
		1297/1301 s	$\nu(C-C)_{inter-ring}$[d]		
1272 w	1270 m		$\delta_{CH} + \nu_{ring}$		
1235 sh[e]	1235 m		unassigned		
		1233 w	$\nu(N^+-CH_3)$		
1222 sh[f]			unassigned		
		1184/1187 m	9a $\delta_{CH} + \nu_{ring}$[g]		
1169 sh					ν_{as}(T−O−T)
1106 sh					ν_{as}(T−O−T)
1040 vs					ν_{as}(T−O−T)
830 vw	846 w		"d"[h]		
817 vw	815 vs		11 γ_{CH}[i]		
	785 w		10a γ_{C-H}		
	707 w		17b γ_{C-H}		
	671 vw		"4"		
		837 m	$\nu_{ring} + \delta_{ring} + \nu_{inter-ring}$		
771 m					ν_s(O−T−O)[j]
725 w					$\nu(AlO_4)$[j]
		605 w			unassigned
		659 w	6b $\delta_{ring} + \nu_{ring}$		
608 m					ν(D6)[j]
		500 m			δ(O−T−O)[k]

Band intensities: vs = very strong, s = strong, m = medium, w = weak, vw = very weak

[a] The bands between ca. 1250 and 900 cm^{-1} are not shown because they are not visible in the MV^{2+}−L zeolite spectrum mainly from masking from the strong ν_{as}(T−O−T) zeolite peak. [b] See ref 38. [c] Many papers originally regarded this vibration as a $\delta(CH_3)$ peak but was reassigned by Poizat et al. as the "14" benzene ring vibration on the basis of deuterium experiments: see ref 42. [d] See ref 70. [e,f] These peaks appear as very weak shoulders in MV^{2+}−L zeolite and are not shown. [g] See ref 62. [h] For an explanation of the "d" vibration, see ref 63. [i] The umbrella CH_3 breathing mode:see ref 64. [j] See refs 50 and 65−67. [k] See ref 68. [l] ν = stretch, δ, γ = in-plane, out-of-plane bend, respectively.

the water bending vibration, the development of a partially hydrated thin MV^{2+}−L zeolite layer ($p = 0.62$) was studied upon evacuation. The result of these experiments is illustrated in Figure 7. It is observed that the height of the 1640 cm^{-1} peak decreases in size with increasing pumping time, while the 1649 cm^{-1} peak nearly remains constant. From this result it follows that the 1640 cm^{-1} band belongs to the water present in the zeolite cavities and that the 1649 cm^{-1} band can be assigned to the MV^{2+}. The water bending peak at 1640 cm^{-1} could not be removed fully by further pumping at room temperature, thus indicating that in thin layer MV^{2+}−L zeolite samples the evacuation of water molecules out of the channels is partly inhibited in contrast to the unloaded zeolite where the water bending vibration can hardly be detected under the same conditions. Therefore, the water peak remaining in Figure 7 after prolonged evacuation is attributed to water molecules hindered from escaping by the MV^{2+}.[32] We observe in Figure 4 for curve 1 that intercalated MV^{2+} in thin layer MV^{2+}−L zeolite samples at low loading is dominated by the presence of a water bending peak at 1640 cm^{-1} that effectively masks the presence of the 8a ring vibration.

The vibrations of MV^{2+} have been investigated by several groups on the basis of spectral correlations.[33−38] Hester and Suzuki[39] performed a normal-mode calculation of the in-plane modes, and Poizat et al.[40−42] established a complete assignment based on the spectra of isotopic-substituted MV^{2+} and different MV^{2+} salts. In its various dihalide salts, the MV^{2+} was found to be planar,[43] whereas in the $PdCl_4^{2-}$ salt and in solution the two pyridyl rings are twisted.[40] The assignment given in Table 3 corresponds predominantly to the one given by Poizat et al.,[40,42] who almost exclusively uses Wilson's notation to describe the pyridyl ring modes.[44−46] According to this, there are five in-plane C−C stretching vibrations: 8a, 8b, 19a, 19b, 14, which are detailed in Table 3. The 6b mode is a radial skeletal vibration, the 4 mode is an out of plane skeletal vibration, and the 9a mode is an in plane C−H bend. All ring vibrations occur twice in MV^{2+}: as an in-phase and an out-of-phase combination of the vibrations of the two rings. The in-phase combinations give stronger peaks in the Raman and the out-of-phase combinations stronger bands in the IR spectra.

It is seen that the intercalation of MV^{2+} causes four of its peaks to show an appreciable shift, viz., peaks 830 vw, 1335 w, 1457 m, and 1570 w cm^{-1}. In comparing the MV^{2+}−L zeolite to the $MVCl_2$−KBr pellet IR spectra in Figures 4 and 5, the disappearance of some bands and these shifts indicate weak interaction between the host zeolite L lattice and the guest MV^{2+}. Examples of guest−host interactions involving MV^{2+} are seen in refs 40 and 47. The analysis of different MV^{2+} salts reported in the literature has shown that some MV^{2+} vibrations are influenced by the conformation of the two pyridyl rings. The mode $\nu(N^+-CH_3)$ especially should only be visible in the Raman spectrum if the two rings are twisted. The low value of

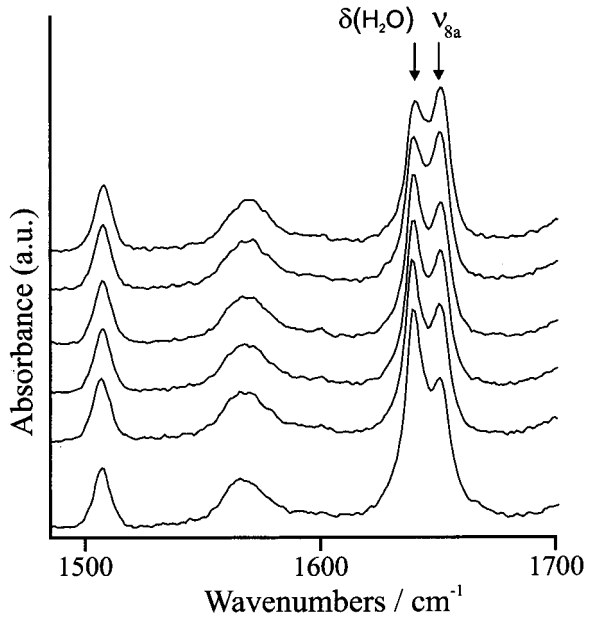

Figure 7. The dependence of the IR bands at 1649 and 1640 cm^{-1} of a thin layer $MV^{2+}-L$ zeolite sample ($p = 0.62$) on the evacuation time. Reading the peaks from bottom to top, the evacuation times for each are 5, 25, 40, 60, 120, and 200 min, respectively.

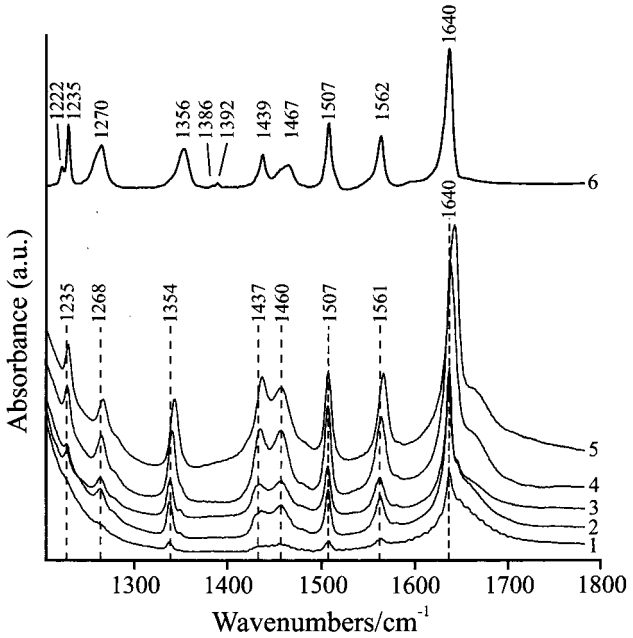

Figure 8. IR spectrum of a $MVCl_2-KBr$ pellet (6) and of $MV^{2+}-Y$ zeolite samples at different loading (1 to 5). The spectra 1 to 5 refer to samples with 1, 5, 9, 12, and 16 MV^{2+} per unit cell, respectively. One zeolite Y unit cell contains eight large cavities.

the mode ν_{14}, which occurs at 1335 cm^{-1} in the IR spectrum of $MV^{2+}-L$ zeolite as well as the weak but well developed peak at 1233 cm^{-1} in the Raman spectrum, which can be assigned to the vibration $\nu(N^+-CH_3)$, both indicate that the two pyridyl rings of $MV^{2+}-L$ zeolite are twisted.[40]

Referring to Figure 6, we see the two Raman peaks appearing at 1184 and 1297 cm^{-1} for low-loading levels show small shifts to 1187 and 1301 cm^{-1} for high loadings. The origin of these small shifts is not clear. Since it could be caused by changes of the refractive index of the material as a function of the loading, an interpretation is not attempted. Some zeolite band positions are known to be influenced by the specific nature of the extraframework cations, caused by the different space they require within the framework and by differences in their electrostatic potentials.[48−51] Maxwell et al. have demonstrated a correlation between IR frequency shifts with varying cations exchanged into the zeolite, for zeolites other than zeolite L.[52] This is also observed in the $\nu_{as}(T-O-T)$ bands in Figure 4, where we observe that a shoulder develops at about 1169 cm^{-1} that becomes more distinct with increasing MV^{2+} loading. This indicates the influence of the intercalated MV^{2+} on the zeolite framework; however, the maxima at 1040 and 1106 cm^{-1} are not affected. The specific effect of the zeolite cavity on the MV^{2+} vibrations is illustrated in Figure 8 where we compare the IR spectra of a $MVCl_2-KBr$ pellet with some $MV^{2+}-Y$ zeolite samples at different loading. For the $MV^{2+}-Y$ zeolite spectra, the 1507 cm^{-1} peak, which is the most reliable peak for quantitative IR work, does not show any shift in its position just like in the spectra for $MV^{2+}-L$ zeolite or $MVCl_2-KBr$ measured spectra. The water bending peak for the $MV^{2+}-Y$ spectra is seen as a broad shoulder on the right-hand side of the 1640 cm^{-1} 8a ring vibration peak, while for the $MV^{2+}-L$ spectra it appears as a separate peak at 1640 cm^{-1}, hence causing the shift of its neighboring 8a ring vibration to 1649 cm^{-1}. A shift of the water bending vibration by a few wavenumbers is encountered frequently in zeolites. A role[32] is played not only by the zeolite framework but also by the cations present, as has been shown e.g., for zeolite A.[53] The 1562 cm^{-1} peak in $MV^{2+}-Y$ zeolite shows negligible shift compared to the $MVCl_2-KBr$, whereas in $MV^{2+}-L$ zeolite this peak shows a shift of 8 cm^{-1}. In Y zeolite, two peaks appear at 1460 and 1437 cm^{-1} and both have a corresponding peak in the $MVCl_2-KBr$ spectrum. In $MV^{2+}-L$ zeolite, they merge into a broad feature 1457 cm^{-1}. The 1392 and 1386 cm^{-1} peaks that are weak in $MVCl_2$ do not seem to appear in either $MV^{2+}-Y$ or $MV^{2+}-L$ zeolite spectra. The 1354 cm^{-1} peak in Y zeolite corresponds with the 1356 cm^{-1} peak in $MVCl_2-KBr$, which shows a large shift by 20 cm^{-1} in $MV^{2+}-L$ zeolite and is seen at 1335 cm^{-1}. The 1268 cm^{-1} peak in $MV^{2+}-Y$-zeolite shows a minor shift away from its 1270 cm^{-1} counterpart in $MVCl_2-KBr$. It appears at 1272 cm^{-1} in $MV^{2+}-L$ but is much weaker. The 1235 cm^{-1} peak appearing in $MVCl_2-KBr$ and $MV^{2+}-Y$ falls into the region, where in $MV^{2+}-L$ zeolite the strong antisymmeteric T−O−T absorption starts to dominate. It, therefore, is not visible in Figure 4.

3.3. Zeolite Framework Vibrations as Internal Standard for Quantitative Analysis. The quantitative evaluation of the vibrational spectra presents an alternative fast and nondestructive method of determining the occupation probability of MV^{2+} loaded zeolite samples. It has been shown that the very strong antisymmetric $\nu_{as}(T-O-T)$ stretching vibration in thin zeolite Y layers on ZnSe can serve as an internal standard, thus allowing measurements which otherwise would have been very difficult.[31] The IR spectra in Figures 4 and 5 as well as the corresponding Raman spectra in Figure 6 indicate that in the IR the four zeolite bands can be considered as possible candidates to act as a reference (1040, 771, 725, and 608 cm^{-1}) while in the Raman spectrum only the 500 cm^{-1} band is suitable. The most reliable IR MV^{2+} band was found to be the relatively sharp ν_{8b} peak at 1507 cm^{-1}, which does not show any deviation in position when compared to its counterpart in a $MVCl_2-KBr$ pellet sample. In the Raman spectrum, several MV^{2+} peaks can be used. The results reported in Figure 9 show the ratio of the IR peak area of the $\nu_{8b}(MV^{2+})/\nu_{as}(T-O-T)$ bands versus the independently determined MV^{2+} loading p (top graph). Also shown are the Raman peak area ratios $\nu_{8a}(MV^{2+})/\delta(O-T-O)$ and $\delta_{9a}(MV^{2+})/\delta(O-T-O)$ versus the MV^{2+} loading p (bottom graph).

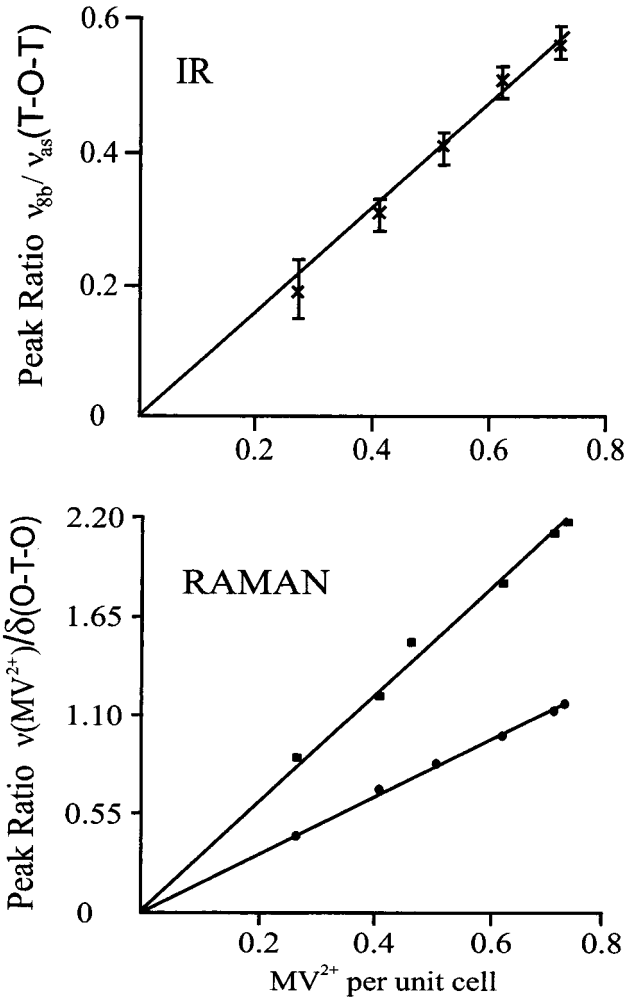

Figure 9. Top graph (concerning IR spectra) shows a correlation between the loading p (MV^{2+} per unit cell) of MV^{2+}−L and the ratio of the area of the $\nu_{8b}(MV^{2+}) = 1507$ cm^{-1} band and the ν_{as}(T−O−T) = 1040 cm^{-1} band. Bottom graph shows the same for the Raman bands $\nu_{8a}(MV^{2+}) = 1651$ cm^{-1} shown by squares (■) and $\delta_{9a}(MV^{2+}) = 1184$ cm^{-1} shown by circles (●) in both cases with respect to the δ(O−T−O) = 500 cm^{-1} zeolite band.

We observe that both kinds of spectra can be used for quantitative purposes. However, the IR sensitivity is limited severely by the weak MV^{2+} signals with respect to the intense zeolite bands. Raman spectra are considerably more sensitive in this case. With thin layers, which in general give superior spectra, quantitative IR measurements become difficult below $p \approx 0.2$. Raman spectra are more sensitive in this case, and $p < 0.1$ is accessible. A possibility to improve the IR sensitivity is to use one of the 771, 725, or 608 cm^{-1} bands because they allow working with thicker layers, whereas under the same conditions the ν_{as}(T−O−T) peak would be saturated. The problem with these bands is that they are relatively broad and not well-separated. An error of about 5% was observed for the 725 and 608 cm^{-1} bands try integrating and comparing them with the ν_{as}(T−O−T). The 771 cm^{-1} is more reliable, the error being about 2%.

3.4. Specific Surface Area Measurements. We report in Figure 10 the nitrogen adsorption isotherms and the BET-plot of the commercial and of the self-synthesized zeolite. Both samples show a type I isotherm according to the classification of Brunauer et al.[54] with completely filled micropores at very low partial pressure. It is well-known that the BET method cannot be used for surface area determination if the solid

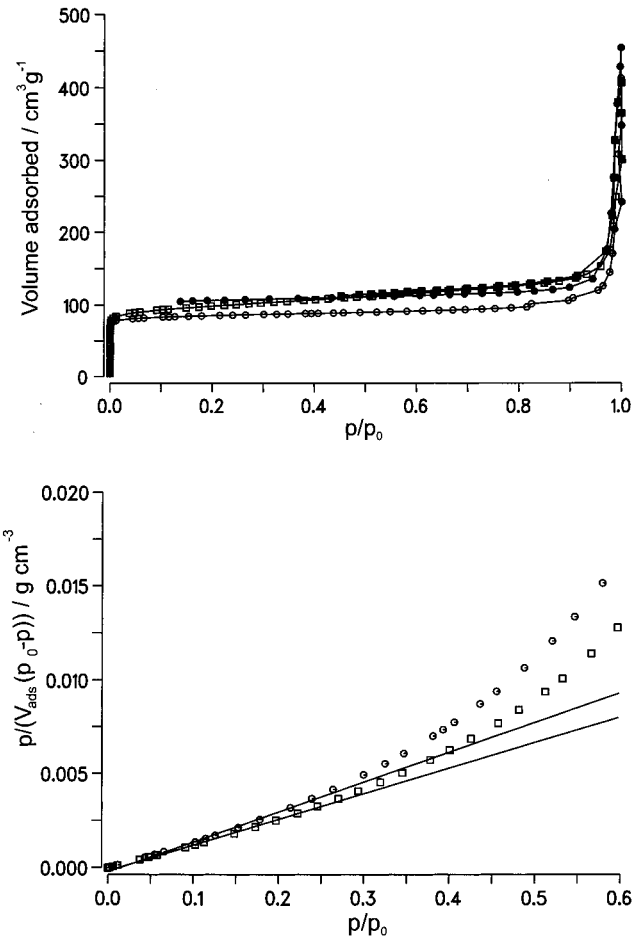

Figure 10. (a) Nitrogen isotherms of commercial zeolite (○) and of self-synthesized zeolite (□). The filled symbols represent the desorption data. (b) BET-plot of commercial (○) and of self-synthesized zeolite (□) in the p/p_0 range of 0.05−0.25.

TABLE 4: Characteristic Data from Adsorption Measurements with Nitrogen at 77 K

adsorbent	n_m(BET) (mL/g)	A_S (BET-area) (m^2/g)	c(BET)	pore specific volume (cm^3/g)
zeolite L (commercial)	64	277	66	0.163
zeolite L (self-synthesized)	74	322	80	0.205

contains pores of molecular dimensions, which is the characteristic of zeolite L.[55,56] For comparative studies of different zeolite L samples, however, it is sufficient to take the calculated BET monolayer equivalent surface area A_s in the region p/p_0 from 0.05 to 0.25, where the BET plot is linear. The characteristic data are listed in Table 4, where n_m is the monolayer capacity and the value c(Bet) is a parameter derived from the BET-theory. We also compare the pore specific volume obtained from the amount adsorbed at a relative pressure at about 0.90 (Gurvich rule) which corresponds to the micropore volume of the sample. The adsorption isotherms and the calculated BET area results confirm the results of MV^{2+} exchange illustrated in Figure 2. The self-synthesized zeolite L sample has a higher specific surface area and a higher micropore volume than the commercial product. This means that there is more accessible pore volume (free space) for the MV^{2+} in the first case.

3.5. Location of the MV^{2+} in Zeolite L by X-ray Structure Refinement and by Molecular Modeling. The Rietveld refinement and modeling of the location of the MV^{2+} in the commercial and self-synthesized L zeolites gave similar results.

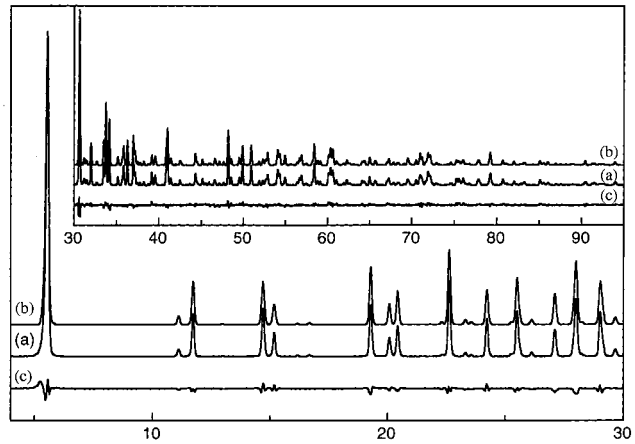

Figure 11. X-ray powder diffraction pattern; scattering intensity versus angle (2Θ/deg). Observed (a), calculated (b) and difference (c) patterns for the Rietveld refinement of the model C of self-synthesized MV^{2+}−L zeolite.

TABLE 5: Models A, B, and C of MV^{2+} Location in Zeolite L[a]

	model A	model B	model C
Z/*N*	2/3	3/4	1/1
Δ (deg)	20.6	24.9	27.2
D (Å)	11.64	9.80; 9.91	7.53

[a] *Z*/*N*, (number of MV^{2+})/(number of L unit cells along *c* axis). Δ, angle between the main MV^{2+} axis and the *c* axis of L *D*, separation $MV^{2+}\cdots MV^{2+}$, assuming periodic location of MV^{2+}.

The refinement of MV^{2+}−L was started with the geometrically idealized coordinates for the framework atoms. The positions of the framework atoms were then refined using high-angle data (2Θ > 30°) and distance and angle constraints. After this refinement, only the data below 2Θ < 30° showed significant intensity differences. The cations K(1), K(2), and K(3) were subsequently located in the series of the difference Fourier maps, and these agree with the positions found in synthetic zeolite L.[57] The Na and K position at ($^1/_3$,$^2/_3$,0) partially occupied in zeolite L,[57] is not occupied in the structure of MV^{2+}−L. Only two partially occupied water positions were found (O(7) and O(8)), which add up to a total water content of about 12 water molecules per unit cell. The positions have a high-displacement parameter, and their coordinates must not be taken as actual positions. The position of the water will vary from unit cell to unit cell and depends on the actual location of the viologen molecule in a specific unit cell. Despite their low population parameters, these water positions were essential for a stable refinement as illustrated in Figure 11.

Molecular modeling with the Cerius package[58] was performed to elucidate possible locations of cations MV^{2+} inside the channel. The geometry of the free MV^{2+} was optimized using the energy minimization tools of the Cerius package (conjugate gradient method). A twist angle around the pyridine−pyridine bond of 39.6° was found. The positions of the maxima in the difference Fourier maps were used to locate the encapsulated MV^{2+} cations inside the main channel. Broad disklike clouds of electron density were found, lying normal to the *c*-axis of the zeolite. These "disks" were used to estimate the angle between the main molecular axis of MV^{2+} and the *c*-axis of zeolite. Further searching was done using molecular modeling. Three models, A, B, and C, were tested (see Table 5) for the location of the cations MV^{2+} inside the channels of zeolite L. All the models A, B, and C may be described in terms of two types of disordering: (1) disordering around the 6-fold axis (the MV^{2+} molecule does not satisfy the high 6-fold symmetry along the channel axis) and (2) disordering along the channel. The first type of disordering is due to the noncoincidence of the point symmetry of the MV^{2+} (not higher than 2) and to the large channel of the zeolite L (6/*mmm*). The second type of disordering is a result of the noncoincidence of the size of the MV^{2+} cation and the period $c = 7.5265$ Å of the zeolite framework. Disordering of the type (1) only has to be invoked for the description of the MV^{2+}−L structure in the model C.

Model A. Two symmetrically independent MV^{2+} molecules are alternating along the zeolite *c* axis with a population $Z/N = 2/3$ (Table 5) and are characterized by an angle of 20.6° between the main MV^{2+} axis and the *c*-axis of the zeolite. This results in a separation between the centers of gravity of the MV^{2+} along the zeolite *c* axis of 11.640 Å. Both MV^{2+} cations are situated on a mirror plane, but only one of the pyridine rings in every molecule satisfies the mirror symmetry because of the torsion between the two pyridine rings. Every MV^{2+} cation is statistically disordered among six positions in the cage. The above-mentioned reduced occupancy of the water positions O(7) and O(8)[57] makes it possible to avoid short contacts to the disordered MV^{2+} cations.

Model B. Three symmetrically independent cations MV^{2+} are alternating along the *c* axis with a population $Z/N = 3/4$. The angle between the main molecular axis of MV^{2+} and the *c*-axis of the zeolite is $\Delta = 24.9°$ and the separations between the centers of gravity of MV^{2+} molecules are $D = 9.80$ and 9.91 Å. Similar to the model A, the MV^{2+} molecules are situated on the mirror planes and statistically disordered around the 6-fold axis.

Model C. The best fit of the observed and calculated structure factors was obtained for the model C with theoretically one MV^{2+} cation per unit cell. For the description of the model C, only a disordering of the MV^{2+} of the type (1) around the 6-fold axis has to be invoked. During the refinement, strong restraints on the distances and angles were applied to the organic cation to make it fairly rigid. Only a weak restraint was placed on the rotation around the central C−C bond. The occupancy factors and isotropic displacement parameters of the complete MV^{2+} were refined; i.e., the population factors of all the atoms of the MV^{2+} cation were constrained to be equal. The refined population parameter of $q = 0.038$ for the MV^{2+} corresponds to a loading of 0.9 molecules per unit cell, in close agreement with the chemical analysis value of 0.85. The final atomic parameters for this model are given in Table 6. The numbering of the atoms is explained in Scheme 2. In Table 7, we report selected bond distances, and the profile fit is shown in Figure 11. Further details of the refinement are also given in Table 2.

In the model C, the MV^{2+} cation is located near the channel wall of the zeolite (see Figure 12). This is the main difference to the models A and B, where the MV^{2+} cations have retained their positions in the center of the channel. The shortest distances between the molecule and the framework oxygens are around 3 Å, indicating possible C−H···O hydrogen bridges. The estimated standard deviations (esd's) of these contacts are approximately 0.5 Å. These large esd's are a result of the disorder and the corresponding difficulty to accurately locate the MV^{2+}. Nevertheless, the refinement was quite sensitive to the exact placement of the MV^{2+}, which is also indicated by the failure of models A and B to give acceptable agreement factors for the X-ray data. Close contacts between organic moieties and the channel wall in a zeolite are to be expected and are the rule rather than the exception. For instance, in the self-synthesized zeolite EMC-2 (EMT), the template molecule

TABLE 6: Atomic Coordinates, Isotropic Displacement Parameters and Population Parameters *q* for Self-Synthesized Zeolite MV^{2+}−L[a]

atom	*x*	*y*	*z*	U_{iso}(Å^2)	*q*
SiAl(1)	0.166(1)	0.4993(9)	0.209(2)	2.3(2)[b]	
SiAl(2)	0.095(1)	0.358(1)	0.5000	2.3(2)	
O(1)	0.265(1)	0.5292	0.253(5)	3.7(5)[c]	
O(2)	0.100(2)	0.412(1)	0.319(2)	3.7(5)[c]	
O(3)	0.1476	0.574(1)	0.270(5)	3.7(5)[c]	
O(4)	0.143(2)	0.473(2)	0	3.7(5)[c]	
O(5)	0	0.273(3)	1/2	3.7(5)[c]	
O(6)	0.163(1)	0.3257	1/2	3.7(5)[c]	
O(7)	0.172(8)	0.910(7)	0.10(1)	12.	0.32(4)
O(8)	0.11(1)	0.13(1)	0.66(2)	20.	0.19(7)
K(1)	1/3	2/3	1/2	4.6(7)[d]	
K(2)	0	0.5000	1/2	4.6(7)[d]	0.90(5)
K(3)	0	0.300(3)	0	4.6(7)[d]	0.50(3)
N(1)	0.07(2)	0.049(9)	0.21(7)	5(2)[e]	0.038(7)[f]
C(2)	0.03(1)	0.097(7)	0.35(8)	5(2)[e]	0.038(7)[f]
C(3)	0.038(6)	0.057(5)	0.51(8)	5(2)[e]	0.038(7)[f]
C(4)	0.101(7)	0.027(4)	0.54(7)	5(2)[e]	0.038(7)[f]
C(5)	0.145(6)	0.073(5)	0.39(7)	5(2)[e]	0.038(7)[f]
C(6)	0.13(2)	0.036(9)	0.22(7)	5(2)[e]	0.038(7)[f]
C(7)	0.07(3)	0.09(1)	0.04(7)	5(2)[e]	0.057(10)[g]
N(11)	0.14(2)	0.143(7)	1.04(7)	5(2)[e]	0.038(7)[f]
C(12)	0.05(1)	0.048(5)	0.82(7)	5(2)[e]	0.038(7)[f]
C(13)	0.06(2)	0.09(2)	1.00(7)	5(2)[e]	0.038(7)[f]
C(14)	0.115(8)	0.068(6)	0.71(7)	5(2)[e]	0.038(7)[f]
C(15)	0.197(9)	0.124(7)	0.77(7)	5(2)[e]	0.038(7)[f]
C(16)	0.21(1)	0.17(1)	0.93(7)	5(2)[e]	0.038(7)[f]
C(17)	0.16(2)	0.18(3)	1.23(7)	5(2)[e]	0.057(10)[g]

[a] Number in parentheses are the esd's. [b−f] Parameters with the same superscript were constrained to be equal. [g] The population parameters for C(7) and C(17) (methyl groups) were multiplied by a factor of 1.5 to account for the protons.

SCHEME 2: Model of MV^{2+} in Zeolite L with the Atoms Numbered

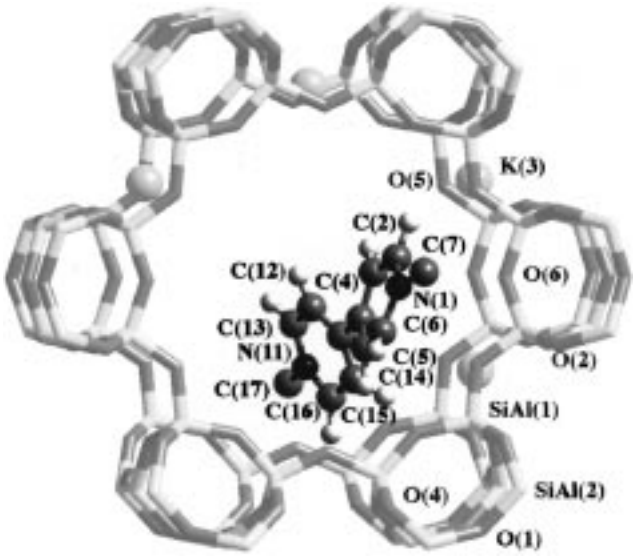

18-crown-6 is also located on the one side of the cage, where it is anchored by three Na^+ cations associated with the 6-rings of the framework.[59] In the structure of a F^--containing $GaPO_4$-LTA, the N-atom of the template dipropylamine is shifted away from the center of the 8-ring by about 0.6 Å, which allowed the formation of strong N−H···O hydrogen bonds to the framework.[60]

The rotation of the methylpyridinium of the MV^{2+} cation around the central C−C bond has changed insignificantly during the refinement to 36.6°. This is very close to the value of 37.79° found for instance in the crystal structure of the complex of iridium(I) maleonitriledithiolate with which MV^{2+} forms an optical charge-transfer complex between the metal anion and itself.[61] As emphasized in ref 61, the majority of crystal structures of charge-transfer complexes of MV^{2+} with both organic and inorganic anions shows a planar structure of the cation MV^{2+}.

TABLE 7: Selected Inter Atomic Distances (Å) and Angles (deg)

SiAl−O	
minimum	1.63(3)
maximum	1.67(3)
average	1.65
SiAl−O−SiAl	
minimum	131(3)
maximum	148(2)
average	140
K−O	
K(1)−O(1)	2.87(2) 6×
K(2) −O(3)	2.92(2) 4×
K(3) −O(4)	2.95(5) 2×
shortest distances MV^{2+}-framework	
C(17)−O(5)	2.8(5)
C(5)−O(6)	3.0(2)
C(15)−O(6)	2.9(4)

4. Conclusions

We have presented a study of the MV^{2+} occupation probability in the channels of zeolite L as a function of MV^{2+} present in an aqueous dispersion for commercially available and for self-synthesized zeolite L microcrystals. Care was taken to remove molecules that were adsorbed on the outer surface. The vibrational spectra (IR and Raman) of such samples were studied at different MV^{2+} loading, and nitrogen adsorption isotherms were measured to obtain information of the specific surface area of the commercial and of self-synthesized material. The location of the MV^{2+} in the zeolite L channels for maximum loading, which was 0.85 for the best samples, was studied by X-ray powder diffraction and by molecular modeling.

The infrared and Raman spectra lead to quantitative and qualitative results. For thin zeolite layers coated on ZnSe wafers, quantitative information can be obtained by using the characteristic antisymmetric ν_{as}(T−O−T) band,[69] T = Si or Al, as an internal standard similary as recently reported for $Mo(CO)_6$ in zeolite Y,[31] despite the fact that the intensity of the MV^{2+} vibrations is very low with respect to the ν_{as}(T−O−T) band. Raman spectra turned out to be more sensitive for quantitative studies of MV^{2+}−L zeolites, the 500 cm^{-1} framework vibration being of similar intensity as the MV^{2+} bands. The low value of the mode ν_{14}, which occurs at 1335 cm^{-1} in the IR spectrum of MV^{2+}−L zeolite as well as the weak but well-developed peak at 1233 cm^{-1} in the Raman spectrum, which can be assigned to the vibration $\nu(N^+-CH_3)$, both indicate that the two pyridyl rings of MV^{2+}−L zeolite are twisted. The specific effect of the zeolite L cavity on the MV^{2+} vibrations was studied by comparing the MV^{2+}−L zeolite IR spectra with a $MVCl_2$−KBr pellet and with some MV^{2+}−Y zeolite samples at different loading. The disappearance of some bands and some IR peak shifts indicate weak interaction between the host zeolite L lattice and the guest MV^{2+}, in agreement with the results of Rietveld refinement of X-ray data and molecular modeling. We found that the angle between the main molecular axis of MV^{2+} and the *c*-axis of the zeolite is 27° with the MV^{2+} lying along the channel wall. This tilt makes it possible to have a cation in each cage, despite the fact that the cation is longer than the repeat distance along the channel of the zeolite L. However,

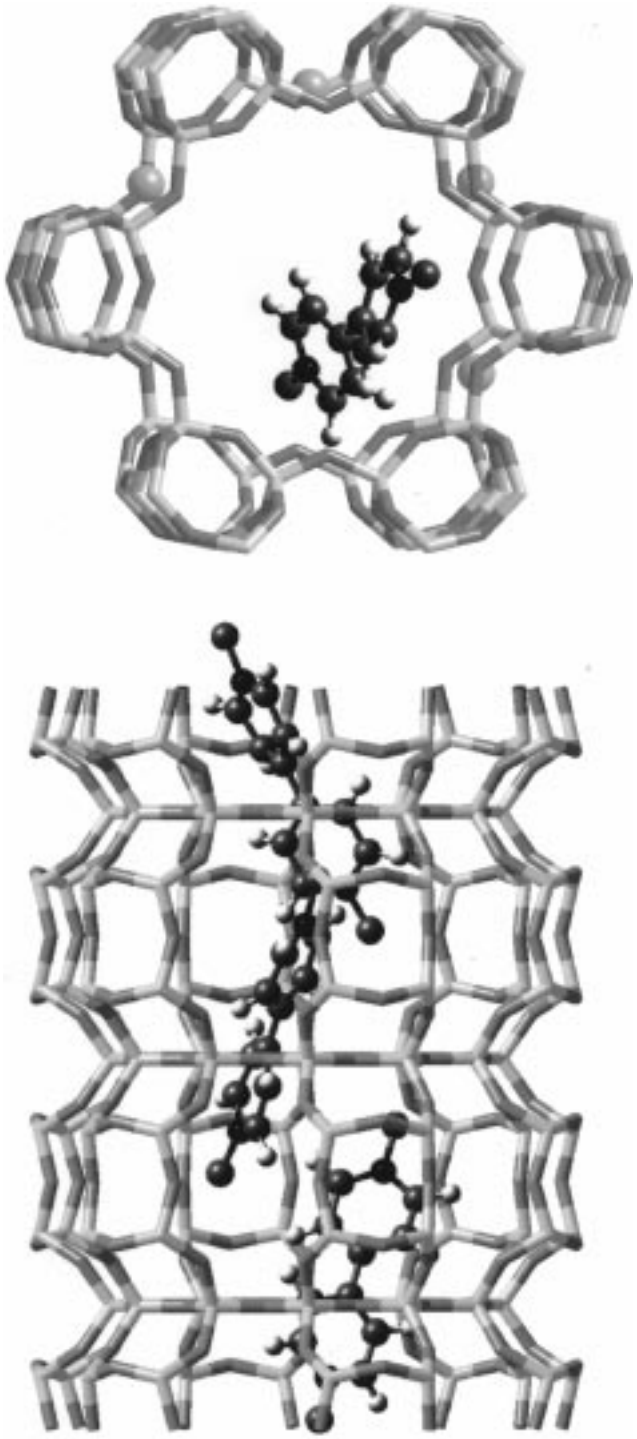

Figure 12. Location of the MV^{2+} cation inside the channel of zeolite L according to model C. Top: view along the channel axis showing one possible position and orientation of a molecule and the atom labeling scheme. The water molecules and the $K^+(4)$ cations too close to this position of the molecule are not shown. Bottom: side view of the channel depicting a likely arragement of the molecules along the one-dimensional channel.

the MV^{2+} cannot be in a periodic chain along the channel axis since the shortest contact distance for this arrangement is 2.4 Å. Neighboring MV^{2+} must, therefore, be rotated around the 6-fold axis, which does increase the distances between the cations. For a rotation of 120° (3-fold screw axis) the intermolecular contacts $MV^{2+}\cdots MV^{2+}$ along the *c* axis have normal values of 3.3−3.4 Å. The close contacts with the channel wall is probably the result of weak MV^{2+} cation−zeolite interactions. We conclude that this detailed study of MV^{2+} intercalated in the channels of zeolite L is a good starting point for improving our understanding of supramoleculary organized dye molecules in the channels of zeolite L.[3−8]

Acknowledgment. This work was supported by the Swiss National Science Foundation, Project NFP 36 (4036-043853), and by the Swiss Federal Office for Energiewirtschaft, Project 10441. In addition, the authors thank Dr. Niklaus Gfeller and Dr. Roman Imhof for fruitful discussion, Mr. Philipp Gut for measuring the MV^{2+}−Y zeolite spectra, Professor R. Giovanoli for providing the SEM photographs, and Messrs René Bühler and René Schraner for their technical support.

References and Notes

(1) Suib, S. L. *Chem. Rev.* **1993**, *93*, 803.
(2) Meier, W. M.; Olson, D. H.; Baerlocher, Ch. In *Atlas of Zeolite Structure Types*; Elsevier: London, 1996.
(3) Gfeller, N.; Megelski, S.; Calzaferri, G. *J. Phys. Chem. B* **1999**, *103*, 1250.
(4) Calzaferri, G. *Chimia* **1998**, *52*, 525.
(5) Gfeller, N.; Megelski, S.; Calzaferri, G. *J. Phys. Chem. B* **1998**, *102*, 2433.
(6) Gfeller, N.; Calzaferri, G. *J. Phys. Chem. B* **1997**, *101*, 1396.
(7) Binder, F.; Calzaferri, G.; Gfeller, N. *Sol. Energy Mater. Sol. Cells* **1995**, *38*, 175.
(8) Binder, F.; Calzaferri, G.; Gfeller, N. *Proc. Ind. Acad. Sci.* **1995**, *107*, 753.
(9) Kalyanasundaram, K. *Coord. Chem. Rev.* **1982**, *46*, 159.
(10) Dutta, P. K.; Ledney, M. *Prog. Inorg. Chem.* **1997**, *44*, 209.
(11) Persaud, L.; Bard, A. J.; Campion, A.; Fox, M. A.; Mallouk, T. E.; Webber, S. E.; White, J. M. *J. Am. Chem. Soc.* **1987**, *109*, 7309.
(12) Li, Z.; Wang, C. M.; Persaud, L.; Mallouk, T. E. *J. Phys. Chem.* **1988**, *92*, 2592.
(13) Yoon, K. B.; Kochi, J. K. *J. Phys. Chem.* **1991**, *95*, 1348.
(14) Yoon, K. B.; Kochi, J. K. *J. Phys. Chem.* **1991**, *95*, 3780.
(15) Kim, Y. I.; Mallouk, T. E. *J. Phys. Chem.* **1992**, *96*, 2879.
(16) Yoon, K. B.; Huh, T. J.; Corbin, D. R.; Kochi, J. K. *J. Phys. Chem.* **1993**, *97*, 6492.
(17) Yoon, K. B.; Huh, T. J.; Kochi, J. K. *J. Phys. Chem.* **1995**, *99*, 7042.
(18) Alvaro, M.; Facey, G. A.; García, H.; García, S.; Scaiano, J. C. *J. Phys. Chem.* **1996**, *100*, 18173.
(19) Alvaro, M.; García, H.; García, S.; Márquez, F.; Scaiano, J. C. *J. Phys. Chem. B* **1997**, *101*, 3043.
(20) Calzaferri, G.; Lanz, M.; Li, J. W. *J. Chem. Soc., Chem. Commun.* **1995**, 1313.
(21) Breck, D. W. In *Zeolite Molecular Sieves*; John Wiley & Sons: New York, 1974.
(22) Calzaferri, G.; Gfeller, N. *J. Phys. Chem.* **1992**, *96*, 3428.
(23) Brühwiler, D.; Gfeller, N.; Calzaferri, G. *J. Phys. Chem. B* **1998**, *102*, 16, 2923.
(24) Baumann, J.; Beer, R.; Calzaferri, G.; Waldeck, B. *J. Phys. Chem.* **1989**, *93*, 2292.
(25) Watanabe, T.; Honda, K. *J. Phys. Chem.* **1982**, *86*, 2617.
(26) Baerlocher, Ch. In *X-ray Rietveld System* XRS-82; ETH Zürich: Switzerland, 1982.
(27) Lainé, P.; Seifert, R.; Calzaferri, G. *New J. Chem.* **1997**, *21*, 453.
(28) Atkins, P. W. In *Physical Chemistry*, 5th ed.; Oxford University Press: Oxford, 1994.
(29) Kunzmann, A.; Seifert, R.; Calzaferri, G. *J. Phys Chem. B* **1999**, *103*, 18.
(30) Barrer, R. M. In *Zeolites and Clay Minerals as Sorbents and Molecular Sieves*; Academic Press: London, 1978.
(31) (a) Müller, B. R.; Calzaferri, G. *J. Chem. Soc., Faraday Trans.* **1996**, *92*, 1633. (b) Müller, B. R.; Calzaferri, G. *Microp. Mesop. Mater.* **1998**, *21*, 59.
(32) Barbosa, L.; Calzaferri, G. *Res. Chem. Intermed.* **1995**, *21*, 1, 25.
(33) Haque, R.; Lilley, S.; Coshow, W. R. *J. Colloid Interface Sci.* **1970**, *33*, 185.
(34) Haque, R.; Lilley, S. *J. Agric. Food Chem.* **1972**, *20*, 57.
(35) Benchenane, A.; Bernard, L.; Théophanides, T. *J. Raman Spectrosc.* **1974**, *2*, 543.
(36) Raupach, M.; Emerson, W. W.; Slade, P. G. *J. Colloid Interface Sci.* **1979**, *69*, 398.
(37) Régis, A.; Corset, J. *J. Chim. Phys.* **1981**, *78*, 687.
(38) Forster, M.; Girling, R. B.; Hester, R. E. *J. Raman Spectrosc.* **1982**, *12*, 36.
(39) Hester, R. E.; Suzuki, S. *J. Phys. Chem.* **1982**, *86*, 4626.

(40) Poizat, O.; Sourisseau, C.; Mathey, Y. *J. Chem. Soc., Faraday Trans. 1* **1984**, *80*, 3257.
(41) Poizat, O.; Sourisseau, C.; Giannotti, C. *Chem. Phys. Lett.* **1985**, *122*, 129.
(42) Poizat, O.; Sourisseau, C.; Corset, J. *J. Mol. Struct.* **1986**, *143*, 203.
(43) Russell, J. J.; Wallwork, S. C. *Acta Crystallogr., Sect. B* **1972**, *28*, 1527.
(44) Wilson, F. B. Jr. *Phys. Rev.* **1934**, *45*, 706.
(45) (a)Varsanyi, G. In *Vibrational Spectra of Benzene Derivatives*; Academic Press: New York, 1969. (b) Varsanyi, G. In *Assignments for Vibrational Spectra of Seven Hundred Benzene Derivatives*, Volumes 1 & 2; Budapest, Hungary, 1974.
(46) Lord, R. C.; Marston, A. L.; Miller, F. *Spectrochim. Acta* **1957**, *9*, 113.
(47) McCall, H. G.; Bovey, R. W.; McCully, M. G.; Merkle, M. G. *Weed Sci.* **1972**, *20*, 250.
(48) Baker, M. D.; Godber, J.; Helwig, K.; Ozin, G. A. *J. Phys. Chem.* **1988**, *92*, 6017.
(49) Dutta, P. K.; Rao, K. M.; Park, J. Y. *J. Phys. Chem.* **1991**, *95*, 6654.
(50) Bärtsch, M.; Bornhauser, P.; Calzaferri, G.; Imhof, R. *J. Phys. Chem.* **1994**, *98*, 2817.
(51) Brémard, C.; Bougeard, D. *Adv. Mater.* **1995**, *7*, 10.
(52) Maxwell, I. E.; Baks, A. *Adv. Chem. Ser.* **1973**, *No. 121*, 87.
(53) See Table II of ref 24.
(54) Brunauer, S.; Emmet, P.; Teller, E. J. *J. Am. Chem. Soc.* **1938**, *60*, 309.
(55) Sing, K. S. W. Reporting Physisorption Data for Gas/Solid Systems. *IUPAC* **1982**, 54, *11*, 2201.
(56) Sing, K. S. W. *J. Porous. Mater.* **1995**, *2*, 5.
(57) Barrer, R. M.; Villiger, H. *Z. Kristallografiya* **1969**, *128*, 22.
(58) Cerius, Release 1.6, Molecular Simulations: Burlington, 1995.
(59) Baerlocher, Ch.; McCusker, L. B.; Chiapetta, R. *Microporous Mater.* **1993**, *2*, 269.
(60) Simmen, A.; Patarin, J.; Baerlocher, Ch. In *Proceedngs of the Ninth International Conference on Zeolites*; von Ballmoos, R., Higgins, J. B., Treacy, M. M. J., Eds.; Montreal, 1992; p 433.
(61) Megehee, E. G.; Johnson, C. E.; Eisenberg, R. *Inorg. Chem.* **1989**, *28*, 2423.
(62) Lu, T.; Birke, R.; Lombardi, J. *Langmuir* **1986**, *2*, 305.
(63) Le Calve, N.; Labarbe, P. *Spectrochim. Acta* **1970**, *26A*, 77.
(64) Bellamy, L. J. In *The Infrared Spectra of Complex Molecules*; Chapman and Hall: London, 1975.
(65) Flanigen, E. M.; Khatami, H.; Szymanski, H. A. *Adv. Chem. Ser.* **1971**, *No. 101*, 201.
(66) Pichat, P.; Franco-Parra, C.; Barthomeuf, D. *J. Chem. Soc., Faraday Trans. 1* **1975**, *71*, 991.
(67) Tai No, K.; Bae, D. H.; Jhon, M. S. *J. Phys. Chem.* **1986**, *90*, 1772.
(68) Angeli, C. L. *J. Phys. Chem.* **1973**, *77*, 222.
(69) Milkey, R. G. *Am. Mineral.* **1960**, *45*, 990.
(70) Lee, P. C.; Schmidt, K.; Gordon, S.; Meisel, D. *Chem. Phys. Lett.* **1981**, *80*, 242.